SLAC-PUB-5008
June 1989
(T/E)

Probing the $WW\gamma$ vertex at a 1 TeV e^+e^- collider using the process $e\gamma \rightarrow W\nu^\star$

ERAN YEHUDAI

Stanford Linear Accelerator Center

Stanford University, Stanford, California 94309

ABSTRACT

We suggest that, at a future TeV-energy linear e^+e^- collider, the process $e\gamma \rightarrow W\nu$ will give an effective measurement of the $WW\gamma$ vertex. By measuring the total cross-section and the forward-backward asymmetry, the couplings κ and λ can be measured to a few percent accuracy.

Submitted to Physical *Review D*

⋆ Work supported by the Department of Energy, contract DE–AC03–76SF00515

I. Introduction

The standard-model is widely accepted as the framework of contemporary high-energy physics. The spinor-vector sector of the theory has been rigorously tested and verified. The vector-vector sector of the theory, however, has not been subject to direct experimental test so far. The couplings of the vector-vector sector are completely determined within the standard-model. Radiative corrections to these couplings in the standard-model have been calculated. From these corrections, which depend on masses of both the top quark and the Higgs boson, the bounds $-2.5 \times 10^{-3} < A_K < 1.5 \times 10^{-2}$ and $-3.5 \times 10^{-3} < \lambda < 2.5 \times 10^{-3}$ were extracted.[1] Some extensions to the standard-model which do not significantly relax these bounds include two Higgs doublet models[2] and supersymmetry[3].

Some "new physics" scenarios consistent with low-energy experiments do, however, suggest significant deviations from the standard-model tree level values. These include composite W's[4] and non-decoupling effects of heavy quark loops.[5]

We suggest using the process $e\gamma \to W\nu$ in the context of a 1 TeV e^+e^- collider to measure these couplings. This process has been studied before,[6] but usually in lower energies and in an "idealized" e-y collider. The consequence of working in a-more realistic setting is discussed below. This process has several advantages over other processes such as $e^+e^- \to W^+W^-$. Considering only $W \to \mu\nu_\mu$ decays, we have a very clean, virtually background free, event topology — a single muon scattering against nothing. The only possible background is from the process $eZ \to W\nu$. The cross-section for this process is smaller by about two orders of magnitude than the one we are considering. The effects of this background will not alter our conclusions in any way, but will have to be taken into consideration in an eventual analysis of the experimental results.

Further, only the $WW\gamma$ vertex contributes; there are no complicating effects of γ-Z interference. The process has a relatively large cross-section, especially if one considers the effect of beamstrahlung (see below), and thus good statistics can be achieved with a realistic luminosity.

In the next section we present our parametrization of the $WW\gamma$ interaction as a Lagrangian with non-standard couplings.[7] In Sec. III we review existing bounds on anomalous couplings from unitarity considerations and low-energy experiments.[8–12] Sec. IV reviews analyses of the capabilities of some purposed future colliders using other processes.[8,9,13] The remainder of the paper presents our analysis proper. In Sec. V we describe the methods used in calculating cross-sections. The effective photon spectrum is discussed in Sec. VI. We present our results in Sec. VII, and summarize our conclusions in Sec. VIII.

II. The Lagrangian

We use the most general C and P conserving $WW\gamma$ interaction term in the Lagrangian [7]:

$$L = -ie\left[W^\dagger_{\mu\nu}W^\mu A^\nu - W^\dagger_\mu A_\nu W^{\mu\nu} + \kappa W^\dagger_\mu W_\nu F^{\mu\nu} + \frac{\lambda}{m_W^2}W^\dagger_{\sigma\mu}W^\mu_\nu F^{\nu\sigma}\right], \quad (11.1)$$

where

$$W_{\mu\nu} = \partial_\mu W_\nu - \partial_\nu W_\mu, \quad F_{\mu\nu} = \partial_\mu A_\nu - \partial_\nu A_\mu. \quad (11.2)$$

An additional term of the form $\epsilon^{\mu\nu\tau\sigma}(W^\dagger_{\sigma\nu}W_\tau - W_\nu W^\dagger_{\sigma\tau})A_\mu$ is CP conserving, but violates C and P separately. Corrections due to heavy fermion loops do give this term a non-zero coefficient: but it is normally ignored in studies of the pure gauge sector.

The parameters κ and λ are related to the magnetic dipole moment μ and the electric quadrupole moment Q of the W boson by

$$\mu = (1 + \kappa + \lambda)\frac{e}{2m_W}, \qquad Q = -\frac{2e}{m_W^2}(\lambda - \kappa). \tag{II.3}$$

In the standard-model, κ = **1** and λ = 0 at the tree level.

The $WW\gamma$ vertex with momenta labeled as in figure 1 is then given by

$$\begin{aligned}\Gamma^{\mu\nu\alpha} = ie\Bigg[& g^{\alpha\nu}\left(p^\mu + \bar{p}^\mu - \frac{\lambda}{m_W^2}(\bar{p}\cdot q)\,p^\mu + \frac{\lambda}{m_W^2}(p\cdot q)\,\bar{p}^\mu\right) \\ & - g^{\alpha\mu}\left(\bar{p}^\nu - \kappa q^\nu - \frac{\lambda}{m_W^2}(p\cdot q)\bar{p}^\nu + \frac{\lambda}{m_W^2}(p\cdot\bar{p})\,q^\nu\right) \\ & - g^{\mu\nu}\left(p^\alpha + \kappa q^\alpha + \frac{\lambda}{m_W^2}(\bar{p}\cdot q)\,p^\alpha - \frac{\lambda}{m_W^2}(p\cdot\bar{p})\,q^\alpha\right) \\ & + \frac{\lambda}{m_W^2}\bar{p}^\mu p^\alpha q^\nu - \frac{\lambda}{m_W^2}p^\mu q^\alpha \bar{p}^\nu\Bigg]\end{aligned} \tag{II.4}$$

In the process $e\gamma \to W\nu$ with momenta as in fig. 2 one can substitute $p \to p_4$, $q \to p_2$, $\bar{p} \to p_4 - p_2$ and take $p_2^2 = 0$, $p_4^2 = m_W^2$. The vertex then takes the form

$$\begin{aligned}\Gamma^{\mu\nu\alpha} = ie\Big[& 2g^{\alpha\nu}p_4^\mu + 2g^{\alpha\mu}p_2^\nu - g^{\mu\nu}(p_4 + p_2)^\alpha + (\kappa - \lambda - 1)(g^{\mu\alpha}p_2^\nu - g^{\mu\nu}p_2^\alpha) \\ & + \frac{\lambda}{m_W^2}(p_2 + p_4)^\alpha\left(p_4^\mu p_2^\nu - (p_4\cdot p_2)\,g^{\mu\nu}\right)\Big].\end{aligned} \tag{II.5}$$

We mainly concern ourselves with the $WW\gamma$ vertex, but at some points we also need to refer to the WWZ vertex. In these cases we use κ_Z and λ_Z as the analogues of κ and λ.

III. Unitarity and Low Energy Constraints

Theoretical, model independent considerations use unitarity arguments to put constraints on the $WW\gamma$ couplings. Unitarity calculations depend on a cutoff scale Λ, presumably related to the scale of the new physics behind the non-standard-model interactions. Baur and Zeppenfeld give[8] the bounds

$$|\Delta\kappa| < \frac{1.86}{\Lambda^2} \quad \text{for } \lambda = 0, \tag{111.1}$$

and

$$|\lambda| < \frac{0.99}{\Lambda^2} \quad \text{for } \kappa = 1, \tag{111.2}$$

where $A_K = \kappa - 1$ and A is in TeV. Kane *et al.* go further,[9] and use the refinement of a correlation between λ and λ_Z to give an independent bound on λ:

$$|\lambda| < 0.6 \quad \text{for A} = 1 \text{ TeV}. \tag{111.3}$$

Current experimental bounds on κ and λ necessarily arise from loop effects, because so far no particle accelerator possesses sufficient energy or luminosity to produce on-shell W's directly. If the $WW\gamma$ vertex deviates from its standard-model value, the resulting theory is not gauge invariant. Therefore the theory cannot be fundamental, but rather must be a low energy approximation of a more basic theory characterized by some (high) energy scale A. Loop calculation results typically depend on that energy scale. Note that the exact result depends on the regularization scheme used in doing the loop integral. Since loop effects from different sources can interfere destructively, these estimates also assume that the non-standard couplings are the only source of new physics in the loop diagram.

Calculating the effects of non standard-model values for κ and λ on the (g − 2) factor of the muon, and comparing to current experimental results, Grau and Grifols get [10]

$$-2.09 < \Delta\kappa \log(\Lambda^2/m_w^2) - \lambda < 5.54. \tag{111.4}$$

Using $e^+e^- \to f\bar{f}$ cross-section data from PETRA, and taking $\lambda = 0$, van der Bifdeduces [11]

$$|\Delta\kappa(\Lambda/m_w)| < 3\,3\,. \tag{111.5}$$

Alcorta *et* al. rely[12] on results from polarization asymmetry in e-D scattering at SLAC, and taking $\lambda = 0$ again, give

$$\left|0.6\Delta\kappa - 0.4(\Delta\kappa)^2\right| < \frac{1}{\Lambda^2} \tag{111.6}$$

(A in TeV.)

Neutrino-nucleon scattering experiments give[9] strong correlation between κ and κ_Z:

$$\left|\Delta\kappa_Z + (\cos\theta_w^2 + \frac{1}{2})\Delta\kappa_z^2 + \sin\theta_w^2\Delta\kappa^2\right| < 0.015\frac{m_W^2}{\Lambda^2}. \tag{111.7}$$

The allowed values form a narrow ellipse-shaped strip in the κ-κ_Z plane. Expressed as an independent bound on κ, one gets for A = 1 TeV approximately

$$|\Delta\kappa| < \frac{1}{2\sin\theta_w\sqrt{\cos\theta_w^2 + 1/2}} = 0.94. \tag{111.8}$$

Data on the heavy boson mass ratio were used by Kane *et al.* to strongly correlate[9] λ and λ_Z. They find (for A = 1 TeV) that one may approximately take $\lambda = \lambda_Z$ for $\lambda, \lambda_Z > 0.15$.

The last two bounds are related to the renormalization of the ρ parameter (p = $m_w^2/m_z^2 \cos\theta_w^2$).

To summarize, the strongest independent bound on κ from low energy experiments is of order 100% (eqn. (III.8)), while the best result on λ is $|\lambda| < 0.6$ (eqn. (111.3)) coming from unitarity considerations.

IV. High Energy Processes

The processes usually considered for measuring the $WW\gamma$ couplings in high-energy colliders are $e^+e^- \to W^+W^-$ in e^+e^- colliders, and $q\bar{q} \to W\gamma$ in $p\bar{p}$ colliders. $e^+e^- \to W^+W^-$ provides a generally sensitive tool for anomalous coupling determination due to cancellations which occur in the standard-model. Using this process is, however, complicated for two reasons. First, WWZ as well as $WW\gamma$ couplings contribute, doubling the number of CP conserving parameters which are apriori independent. Second, the experimental signature is richer, allowing more information to be extracted from individual events. In particular, using the semi-leptonic decay mode (one W decaying leptonically, while the other decays hadronically), information can be gained on the polarization of the W's, at least on a statistical level.

In an e^+e^- collider with a center-of-mass energy of 400 GeV and an integrated luminosity of about $5 \times 10^3 \text{pb}^{-1}$, the bounds

$$-0.11 < \lambda < 0.10, \quad -0.15 < A_K < 0.35 \qquad \text{(IV.1)}$$

are obtainable[9]. ($\lambda = \lambda_z$ which is suggested from low energy experiments was used in obtaining the bound on A_K.) Ahn et al. argue[14] that using the angular

distribution of the W^+W^- pairs in a 1 TeV e^+e^- collider, assuming $\lambda = 0$, the bound $|\Delta\kappa| < 0.03$ can be achieved.

In $p\bar{p}$ colliders, the process of choice is $q\bar{q} \to W\gamma$. It has the advantage over $e^+e^- \to W^+W^-$ in that only the $WW\gamma$ couplings contribute to the process. To avoid backgrounds, only leptonic W decays may be considered. Using that process, very strong bound on λ, of order 1(2)% can be achieved[9] in the proposed SSC (LHC). This strong constraint is possible because λ multiplies a term that grows as $\hat{s}/m_w^2$ where $\hat{s}$ is the invariant mass squared of the W-y system. On the other hand, the best bounds on κ are only of order 10(20)%. The machine parameters considered are center of mass energy of 40 (17) TeV, and integrated luminosity of 10^4pb^{-1}. Other authors[8,13] give similar results.

V. Cross-Section Calculations

Two Feynman diagrams contribute to the process $e\gamma \to W\nu$ (figure 3). The matrix element is given by

$$i\mathcal{M} = \epsilon_\mu^\lambda(p_2)\epsilon_\nu^{\lambda'}(p_4)\mathcal{M}^{\mu\nu}, \tag{V.1}$$

where

$$\begin{aligned} i\mathcal{M}^{\mu\nu} =& \bar{u}_L(p_3)\left(e^2\gamma^\nu\frac{(\not{p}_1+\not{p}_2)}{s}\gamma^\mu + \frac{e\gamma_\sigma\Gamma^{\mu\sigma\nu}}{t-m_w^2}\right)u_L(p_1) \\ =& e^2\bar{u}_L(p_3)\Bigg\{\gamma^\nu\frac{(\not{p}_1+\not{p}_2)}{s}\gamma^\mu + \frac{\gamma_\tau}{t-m_w^2}\Big[2g^{\tau\nu}p_4^\mu + 2g^{\tau\mu}p_2^\nu - g^{\mu\nu}(p_2+p_4)^\tau + \\ & (\kappa-\lambda-1)(g^{\tau\mu}p_2^\nu - g^{\mu\nu}p_2^\tau) + \frac{\lambda}{m_w^2}(p_2+p_4)^\tau(p_2^\nu p_4^\mu - (p_2\cdot p_4)g^{\mu\nu})\Big]\Bigg\}u_L(p_1), \end{aligned} \tag{V.2}$$

$s = (p_1+p_2)^2$, $t = (p_3-p_1)^2$, $\epsilon_\mu^\lambda(p_2)$ and $\epsilon_\nu^{\lambda'}(p_4)$ are the polarization four-vectors

of the photon and the W respectively and $\Gamma^{\mu\sigma\nu}$ is the $WW\gamma$ vertex discussed above.

To account for the distribution of the electron-photon center-of-mass energy, we introduce the effective luminosity $\mathcal{L}_{e\gamma}(\hat{s})$. $\mathcal{L}_{e\gamma}(\hat{s})$ is a dimensionless quantity, defined as follows: the luminosity for an electron-photon collision with center-of-mass energy squared between $\hat{s}$ and $\hat{s}+d\hat{s}$ is equal to $\mathcal{L}_{e\gamma}(\hat{s})(d\hat{s}/s)$ times the overall collider luminosity. The corresponding effective luminosity used here is discussed in detail in the next section.

In terms of the effective luminosity $\mathcal{L}_{e\gamma}(\hat{s})$, the cross-section for WY production is

$$\begin{aligned}\sigma &= \int d\Omega\ (d\hat{s}/s)\mathcal{L}_{e\gamma}(\hat{s})\frac{(2\pi)^4}{2\hat{s}}\left|\sum_{\lambda,\lambda'}\epsilon_\mu^\lambda(p_2)\epsilon_\nu^{\lambda'}(p_4)\mathcal{M}_{\mu\nu}\right|^2\frac{(1-m_W^2/\hat{s})}{8(2\pi)^6} \\ &= \frac{1}{32\pi}\int_{m_W^2}^{s}(d\hat{s}/s)\frac{(1-m_W^2/\hat{s})}{\hat{s}}\mathcal{L}_{e\gamma}(\hat{s})\int_{-1}^{1}d(\cos\theta)\left|\sum_{\lambda,\lambda'}\epsilon_\mu^\lambda(p_2)\epsilon_\nu^{\lambda'}(p_4)\mathcal{M}_{\mu\nu}\right|^2 .\end{aligned} \tag{V.3}$$

The matrix elements were calculated using spinor techniques.[15] These involve calculating the matrix element for each Feynman diagram and polarization combination separately, rather than averaging over polarizations. These techniques are particularly convenient in our case because they greatly simplify the treatment of the W decay into fermions, and because all the fermions in the problem can be taken to be massless.

Following reference 15 we explicitly sum over photon polarizations. The sum over W polarizations is replaced by an integral over what is effectively the direction of the W decay products. This last step serves as more than computational

convenience. Assuming the W decays into two massless fermions, one may use the matrix elements given in the Appendix as the matrix elements for the process $e\gamma \to \mu\nu_\mu\nu_e$ provided we add a factor of the $W \to \mu\nu_\mu$ branching ratio.

We perform the complete integral over phase space, cutting-off only those events in which the muon direction is less than 10° from the beam pipe. No cut is done on the muon energy, which ranges from the muon mass to half the collider energy. (See fig. 4.) Both $e^+\gamma$ and e-y originated processes are considered.

We neglect diagrams for $e\gamma \to \mu\nu_\mu\nu_e$ in which the μ-ν_μ do not originate from a W, and all the effects associated with the non-zero width of the outgoing W. These diagrams are at least an order of magnitude smaller than those we are considering. Their exclusion does not effect our conclusions, since these depend only on the approximate cross-section, and its sensitivity to the anomalous couplings. These diagrams will, however, have to be included in-a careful analysis of the experimental data.

Nonetheless, we make no approximations with regard to the incoming W. In particular we do not use the effective W approximation.

The full expression for $\left|\sum_{\lambda,\lambda'} \epsilon_\mu^\lambda(p_2)\epsilon_\nu^{\lambda'}(p_4)\mathcal{M}_{\mu\nu}\right|^2$ is given in the Appendix.

VI. The Photon Spectrum

Radiated photons play a very significant role in a TeV scale e^+e^- collider. Although classical bremsstrahlung remains important, a much larger effect [16] arises from the synchrotron radiation emitted by electrons in one beam due to the electric field it experiences as it passes through the other beam; this radiation is termed "beamstrahlung".

Classical bremsstrahlung depends only on the beam energy, and is parametrized to first order by the Weizsacker-Williams distribution functions

$$f(x) \quad \frac{\alpha \log(s/m_e^2)}{2\pi} \frac{1 + (1-x)^2}{x} \tag{VI.1}$$

where x is the fraction of the electron energy carried by the photon. Ordinarily, one neglects the electron energy loss due to bremsstrahlung. When considering beamstrahlung, on the other hand, this is not allowed. The energy loss has to be fully taken into consideration.'

The effect of beamstrahlung cannot be decomposed into distribution functions. We parametrize beamstrahlung in terms of a luminosity function $\mathcal{L}_{e\gamma}(\hat{s})$ as discussed in the previous section. Beamstrahlung depends strongly on machine parameters such as luminosity, pulse rate and bunch geometry.[17,18] Here we use the following set of accelerator parameters, with the terminology as in reference. 18:

$$\text{C} = 0.3, \quad \text{G} = 5.00, \quad Y = 1600. \tag{VI.2}$$

These correspond to a bunch length $\ell_0 \sim 0.4mm$, and a luminosity per pulse $\mathcal{L} \sim 10^{31} cm^{-2}$ (to determine the physics luminosity, multiply $\mathcal{L}$ by the repetition rate, of order $100/\text{sec.}$). The cross-section of the bunches is assumed to be elliptical with a, and a_y as the semi-major and semi-minor axes, and a_x/a_y = 100. Figure 5 shows the corresponding effective luminosity function, with and without beamstrahlung.

Since the amount of radiated energy depends sensitively on the parameters of the machine that is actually constructed, we calculate all our results twice, both with and without including the effects of beamstrahlung. Since the beamstrahlung

spectrum we use here is probably an over-estimate of the amount of radiated energy, the actual results are likely to be somewhere in between the two calculations.

Previous authors[6] who considered the process $e\gamma \rightarrow W\nu$ have pointed out that a radiation zero occurs, provided the couplings take their standard-model values. The cross-section for all helicity combinations is exactly zero when the W scatters forwards (i.e. in the incoming electron's direction). The differential cross-section in the e-y center-of-mass frame is very strongly peaked for W's scattering in the backward direction (figure 6). Since this radiation zero exists only for standard model couplings, the cross-section for forwards scattering W's could be a very sensitive probe for non standard-model couplings.

However, in an e^+e^- collider, the average electron energy is much larger than the average photon energy, and thus the laboratory frame is boosted in the electron's direction with respect to the e-y center of mass frame. The entire W angular distribution is therefore shifted in the forward direction, completely obscuring the radiation zero. The amount of this shift is sensitive to the actual photon spectrum. An additional smearing effect is caused by the fact that, considering only the leptonic W decay mode, its momentum is not reconstructible; only the muon's momentum is known. Figure 7 presents the angular distribution of the detected muons in the laboratory frame. The radiation zero is completely washed away.

Since the absolute cross-section for the process is also sensitive to the photon spectrum, the question of measuring this spectrum with sufficient accuracy becomes prominent. As it turns out, Compton scattering provides a simple yet effective method for measuring the photon spectrum. It provides both a large cross-section and therefore good statistics, and a virtually background free event topology. The process $e\gamma \rightarrow e\gamma$, with both final particles visible and no missing

perpendicular momentum has no background beyond radiative corrections. Furthermore, the momenta of the incoming particles can be reconstructed completely. The cross-section for $e\gamma \to e\gamma$ is

$$d\sigma = 2\pi\alpha^2 \mathcal{L}_{e\gamma}(\hat{s})(d\hat{s}/s) \int \frac{5}{} + \frac{2\cos\theta}{1+\cos\theta} + \frac{\cos^2\theta}{} d(\cos\theta). \qquad \text{(VI.3)}$$

The infra-red divergence is avoided by cutting-off the θ integral at some finite θ_0. This is justified since, experimentally, no detection is possible for small beam-particle angles.

Cross-sections are presented in units of R, where

$$1R = \frac{4\pi\alpha^2}{3s} = \frac{86.8 \text{ fb}}{(E_{\text{CM}}(\text{TeV}))^2}. \qquad \text{(VI.4)}$$

In a 1 TeV e^+e^- collider with an integrated-luminosity of 30fb^{-1}, .one unit of R corresponds to about 2500 events. In these units, one gets

$$d\sigma(\hat{s}) = \mathcal{L}_{e\gamma}(\hat{s})\frac{d\hat{s}}{\hat{s}} \cdot 3\left(\cos\theta_0 + 2\log\left(\frac{1+\cos\theta_0}{1-\cos\theta_0}\right)\right) \qquad \text{(VI.5)}$$

where θ_0 is the minimal angle from the beam direction in which particles can be detected. Equation (VI.5) allows a straightforward determination of $\mathcal{L}_{e\gamma}(\hat{s})$ by measuring the cross-section for $e\gamma$ production in a given $\hat{s}$ bin.

VII. Results

In estimating possible bounds on the anomalous couplings we assume that standard-model results are measured. We then ask what region of the κ-λ plane is consistent with these results to within one standard-deviation

In the calculations presented here we concentrated on the $W \rightarrow \mu\nu_\mu$ decay mode because this is the only mode that gives a completely pure signal. The decay $W \rightarrow \tau\nu$ can also be used as a good source of signal provided the τ can be reliably reconstructed from its decay products. Other decay modes suffer from some backgrounds: $e\gamma \rightarrow eZ \rightarrow e\nu\bar{\nu}$ is a background to the $W \rightarrow e\nu$ decay channel, while $e^+e^- \rightarrow q\bar{q}Z \rightarrow q\bar{q}\nu\bar{\nu}$ is a background to the hadronic W decay modes. If these backgrounds are taken into consideration, one may consider these decay channels as well, thus increasing the total number of available events by a factor of 8. As mentioned above, the only cuts that we impose are that all the visible particles (i.e. the muon in $e\gamma \rightarrow W\nu \rightarrow \mu\nu_\mu\nu_e$ and both electron and photon in $e\gamma \rightarrow e\gamma$) are at least 10^o away from the beam pipe.

The most sensitive probe to the anomalous couplings is the total $W\nu$ production cross-section. The results for the total-cross section for $e\gamma \rightarrow W\nu_e \rightarrow \mu\nu_\mu\nu_e$ as a function of κ and λ are given in the Appendix. Figure 8 shows the total cross-section for $e\gamma \rightarrow W\nu_e \rightarrow \mu\nu_\mu\nu_e$ as a function of κ for several values of λ, while Figure 9 shows its dependence on λ for several values of κ.

In measuring the total cross-section, one has to consider both systematic and statistical errors. The relative statistical error in measuring the total cross-section is

$$\frac{\Delta\sigma(W\nu)}{\sigma(W\nu)} = \frac{1}{\sqrt{N(W\nu)}} = \frac{1}{50\sqrt{\sigma(W\nu)}} \qquad \text{(VII.1)}$$

where $N(W\nu)$ is the total number of W-ν events detected, and σ is measured in units of R.

In addition, one has to consider the statistical errors introduced to $e\gamma \rightarrow W\nu$ cross-section measurements due to the statistical uncertainty in determining the photon spectrum. We make the assumption that one can divide the $\hat{s}$ range into a number of bins such that, while it is still reasonable to take the luminosity function to be constant within each bin, there are enough $e\gamma$ events in each bin so that one can treat their number as having a normal distribution rather than a Poison distribution. Under this assumption, the statistical error in counting W-ν events is adjusted to

$$\frac{\Delta\sigma(W\nu)}{\sigma(W\nu)} \quad \sqrt{\frac{1}{N(W\nu)} + \frac{1}{N(e\gamma)}}, \qquad \text{(VII.2)}$$

where $N(e\gamma)$ is the *total* number of e-y events detected.

The total cross-section for $e\gamma \rightarrow e\gamma$ is 18.8 (5.5), while the standard-model cross-section for $e\gamma \rightarrow W\nu$ is 18.2 (5.1) units of R with (without) beamstrahlung. The statistical error is therefore only 0.0066 (0.012) with (without) beamstrahlung. The systematic errors in measuring the total cross-section do not, however, diminish with the big sample size. Many factors go into decreasing the experimental accuracy, including estimating the detector acceptance and the triggering efficiency. We expect[19] this accuracy to be about 3%.

Additional information can be extracted by measuring the forward - backward asymmetry. As seen in figures 10 and 11, the forward-backward asymmetry is relatively insensitive to small deviations from the standard model values of κ and λ.

The forward-backward asymmetry has, however, the advantage that many of the systematic errors in its measurement cancel. One does have to consider the problem of correctly identifying the muon charge. The typical muon energy is 50-200 GeV (see fig. 4), and so charge misidentification will occur with less than 0.2% probability.[20]

In considering this charge misidentification problem, other systematic errors and the statistical uncertainty, we assume that the forward-backward asymmetry can be measured with an accuracy of 1%.

VIII. Conclusion

The regions in the κ-λ plane which would be excluded if standard-model results are actually measured, are shown in fig. 12(13) with (without) the effects of beamstrahlung. Relying on the total cross-section and the forward-backward asymmetry? only weak bounds (0.05 or weaker) can be put on A_K and λ independently.

Combined with other experimental results, particularly the high accuracy measurement of λ possible in the SSC, an independent bound on κ, of order 3%, is possible. While still outside the range of standard-model radiative corrections, this measurement could give a high lower-bound on the speculated scale of W compositeness.

ACKNOWLEDGMENTS

I am grateful to M. Peskin for many instructive discussions, and for critically reading the manuscript. I would also like to thank Y. Nir for reading the manuscript, and D. Burke for discussing the experimental implications of this work.

APPENDIX

The main ingredient in using spinor techniques are the spinor products

$$s(n,m) = \bar{u}_R(p_n)u_L(p_m), \quad t(n,m) = \bar{u}_L(p_n)u_R(p_m). \tag{A.1}$$

These satisfy

$$\begin{aligned} s(n,m) &= -s(m,n),\ t(n,m) = -t(m,n), \\ s(n,m)^* &= t(m,n), \quad t(n,m)^* = s(m,n), \\ s(n,m)t(m,n) &= 2(p_n \cdot p_m), \end{aligned} \tag{A.2}$$

and more generally

$$s(n_1,n_2)t(n_2,n_3)\cdots s(n_{i-1},n_i)t(n_i,n_1) = \mathrm{Tr}\left\{\frac{1+\gamma_5}{2}\, \not{p}_1\, \not{p}_2 \cdots \not{p}_i\right\}. \tag{A.3}$$

Following the prescription of reference 15, we substitute

$$\epsilon_\mu^\lambda(p_2) \to \frac{\bar{u}_\lambda(p_1)\gamma_\mu u_\lambda(p_2)}{\sqrt{s}} \tag{A.4}$$

for the photon polarization, and replace the summation over W polarizations with an integral:

$$\sum_\lambda \epsilon_\lambda^\nu \epsilon^{*\lambda}_{\nu'} \to \frac{3}{8\pi m_W^2} \int d\Omega_{56}^* \left\{\bar{u}_L(p_5)\gamma_\nu u_L(p_6)\right\} \left\{\bar{u}_L(p_5)\gamma_{\nu'} u_L(p_6)\right\}^*, \tag{A.5}$$

where $p_4 = p_5 + p_6$, $p_5^2 = p_6^2 = 0$, and Ω_{56}^* designates the direction of p_5 in the W center-of-mass frame. After some reordering, and making intensive use of

eqs. (A.2)–(A.3) we have

$$\left|\sum_{\lambda,\lambda'}\epsilon_\mu^\lambda(p_2)\epsilon_\nu^{\lambda'}(p_4)\mathcal{M}_{\mu\nu}\right|^2 = \frac{3}{8\pi m_W^2}\int d\Omega_{56}^*\left(|\mathcal{M}_L|^2+|\mathcal{M}_R|^2\right), \tag{A.6}$$

where

$$\begin{aligned}\mathcal{M}_L = \frac{e^2}{\sqrt{s}}&\Big[(u+(\kappa-\lambda)s)s(6,2)-s(6,1)t(1,3)s(3,2)\Big]t(3,5)\\ &+\frac{\lambda}{2m_W^2}s(2,1)s(6,2)\left(u\,t(1,3)t(5,2)+(t-m_W^2)t(3,2)t(1,5)\right)\end{aligned} \tag{A.7}$$

and

$$\begin{aligned}\mathcal{M}_R = \frac{e^2}{\sqrt{s}}&\Big[s(1,3)t(3,5)+(\kappa-\lambda-1)s(1,2)t(2,5)\Big]t(3,2)s(6,1)\\ &-\frac{\lambda}{2m_W^2}t(3,2)s(2,1)t(2,4)\left(s(2,6)t(2,3)s(3,1)+(t-m_W^2)s(6,1)\right),\end{aligned} \tag{A.8}$$

are the matrix elements for left- and right-handed photons respectively. s, t and u are the usual Lorentz invariants:

$$s=(p_1+p_2)^2,\quad t=(p_1-p_3)^2\quad\text{and}\quad u=(p_3-p_2)^2. \tag{A.9}$$

One could use eqn. (A.3) to analytically calculate $|\mathcal{M}|^2=|\mathcal{M}_L|^2+|\mathcal{M}_R|^2$ in terms of four-vector products, but the results are cumbersome and not illuminating. Further, numerically it is advantageous to calculate $\mathcal{M}_L$ and $\mathcal{M}_R$ directly.

The (complex) numbers $s(n,m)$ and $t(n,m)$ can be calculated numerically

using the following prescription[15]. Choose k_0 and k_1 to be four-vectors such that

$$k_0 \cdot k_0 = 0, \qquad k_1 \cdot k_1 = -1, \qquad k_0 \cdot k_1 = 0 \tag{A.lO}$$

and k_0 is not collinear with any other four-vector in the problem. $s(n,m)$ is then given by

$$s(n,m) = \frac{(p_n \cdot k_0)(p_m \cdot k_1) - (p_n \cdot k_1)(p_m \cdot k_0) - i\epsilon_{\mu\nu\tau\sigma} k_0^\mu k_1^\nu p_n^\tau p_m^\sigma}{\sqrt{4(p_n \cdot k_0)(p_m \cdot k_0)}} \tag{A.ll}$$

An appropriate choice for k_0 and k_1 can significantly simplify this last equation. Taking, for instance,

$$\begin{aligned} p_i^\mu &= (p_i^0, p_i^x, p_i^y, p_i^z) \\ k_0 &= (1,1,0,0) \\ k_1 &= (0,0,1,0), \end{aligned} \tag{A.12}$$

eqn. (A.ll) takes the form

$$s(n,m) = (p_n^y + ip_n^z)\sqrt{\frac{p_m^0 - p_m^x}{p_n^0 - p_n^x}} - (p_m^y + ip_m^z)\sqrt{\frac{p_n^0 - p_n^x}{p_m^0 - p_m^x}}. \tag{A.13}$$

$t(n,m)$ is obtained by complex conjugating (eqn. (A.2)).

The final, numerical results for the total cross-section for the process $e\gamma \to W\nu_e \to \mu\nu_\mu\nu_e$ after integrating over the phase-space and the photon spectrum as a function of $\Delta\kappa = \kappa - 1$ and λ, is

$$\sigma(R) = 18.19 + 39.26\Delta\kappa + 39.03\Delta\kappa^2 + 58.42\Delta\kappa + 133.18\Delta\kappa\lambda + 164.96\lambda^2 \tag{A.14}$$

with beamstrahlung, and

$$\mathbf{a(R) = 5.09} + 10.79\Delta\kappa + 11.74\Delta\kappa^2 + 16.10\lambda + 40.49\Delta\kappa\lambda + 62.19\lambda^2 \qquad \text{(A.15)}$$

without beamstrahlung. These results are the combination of both $e^+\gamma$ and e-y originated processes, cutting-off those events in which the muon direction (in the laboratory frame) is less than 10° from the beam pipe.

REFERENCES

1. G. Couture and J.N. Ng, *Z. Phys.* **C35**(1987), 65.
2. G. Couture *et al.*, *Phys. Rev.* **D36**(1987), **859.**
3. T.M. Aliyev, *Phys. Lett.* **155B**(1985), **364;**
   S. Alam, S.N. Biswas and A. Goyal, *Phys.* Rev. **D33**(1985), **168;**
   G. Couture et *al.*, *Phys. Rev.* **D38**(1988), **860.**
4. T.G. Rizzo and M.A. Samuel, *Phys. Rev.* **D35**(1987), **403;**
   M. Suzuki, *Phys. Lett.* **153B**(1985), 289.
5. C. Ahn *et al.*, *Nucl. Phys.* **B309**(1988), **221.**
6. I.F. Ginzburg et *al.*, *Nucl. Phys.* **B228**(1983), **285;**
   K.O. Mikaelian, *Phys.* Rev. **D30**(1984), 1115;
   J.A. Robinson and T.G. Rizzo, *Phys. Rev.* **D33**(1986), **2608;**
   G. Couture, S. Godfrey and P. Kalyniak GIPP 88-6.
7. H. Aronson, *Phys. Rev.* **186**(1969), **1434.**
8. U. Baur, D. Zeppenfeld, *Phys. Lett.* **B201**(1988), **383.**
9. G.L. Kane, J. Vidal and C.P. Yuan, *Phys.Rev.* **D39**(1989), **2617.**

10. A. Grau and J.A. Grifols, *Phys. Lett.* **B154**(1989), 283.

11. J.J. van der Bij, *Phys.* Rev. **D23**(1987), 1088.

12. R. Alcorta, J.A. Grifols, S. Peris, Mod. *Phys. Lett.* **A2**(1987), 23.

13. U. Baur, CERN-TH-5243/88.

14. C. Ahn *et.al.*, SLAC-Report-329 (1988).

15. R. Kleiss, W.J. Stirling, *Nucl.Phys.* **B262**(1985), 235.

16. G.J. Feldman, in *Proceedings of the Fifteenth SLAC Summer Institute on Particle Physics*, E.C. Brennan, ed. SLAC Report No. 328 (1987).

17. P.B. Wilson, SLAC-PUB-3985 (1986);
R. Blankenbecler and S.D. Drell, *Phys. Rev.* **D36**(1987), 277;
P. Chen, in *Proceedings of the Workshop on Physics at Future Accelerators*, La Thuile(Italy) and-Geneva(Switzerland) CERN 87-07 (1987).

18. R. Blankenbecler and S.D. Drell, *Phys. Rev.* **D37**(1988), 3308.

19. D.L. Burke, private communication

20. R.J. Van Kooten, private communication.

FIGURE CAPTIONS

1) The general $WW\gamma$ vertex.

2) Momenta used in $e\gamma \to W\nu$.

3) Feynman diagrams contributing to $e\gamma \to$ WY.

4) The muon energy distribution in the laboratory frame. The muon energy is given as a fraction of the total collider energy. The solid curve was calculated using the beamstrahlung photon spectrum discussed in Sec. VI, while the dashed curve was calculated using only the classical, Weizsacker-Williams distribution.

5) Effective e-y luminosity as a function of $\hat{s}/s$, where $\hat{s}$ is the center-of-mass energy squared of the e-y system, s is the total center-of-mass energy squared of the collider. The solid line includes the effects of beamstrahlung, the dashed line is the classical bremsstrahlung spectrum.

6) Differential cross-section for $e\gamma \to W\nu$ in the e-y center-of-mass frame.

7) Angular distribution of the muons produced by $e\gamma \to W\nu_e \to \mu\nu_\mu\nu_e$ in the laboratory frame.

8) Total cross-section for $e\gamma \to W\nu_e \to \mu\nu_\mu\nu_e$ as a function of κ for $\lambda = -0.2, 0, 0.2$, with (solid) and without (dashed) beamstrahlung.

9) Total cross-section for $e\gamma \to W\nu_e \to \mu\nu_\mu\nu_e$ as a function of λ for $\kappa = 0.8, 1, 1.2$, with (solid) and without (dashed) beamstrahlung.

10) Forward-backward asymmetry as a function of λ for $\kappa = 1$, with (solid) and without (dashed) beamstrahlung.

11) Forward-backward asymmetry as a function of κ for $\lambda = 0$, with (solid) and without (dashed) beamstrahlung.

12) Regions in the κ-λ plane excluded (shaded) by the total cross-section and forward-backward asymmetry measurements, and calculated with beamstrahlung. Curves corresponding to errors of 3% (solid) and 10% (dashed) in the total cross-section, and 1% in the forward-backward asymmetry are presented. The dotted lines correspond to the 1% measurement of λ possible in the SSC.

13) Regions in the κ-λ plane excluded (shaded) by the total cross-section and forward-backward asymmetry measurements, and calculated without beamstrahlung. The meaning of the curves is the same as in fig. 12.

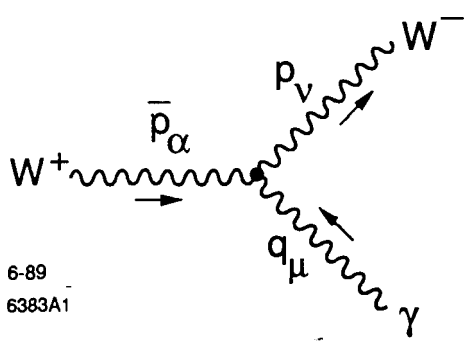

Fig. 1

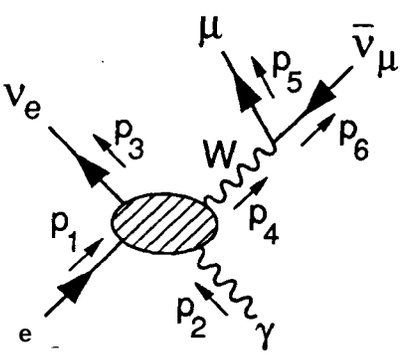

6-69 6383A2

Fig. 2

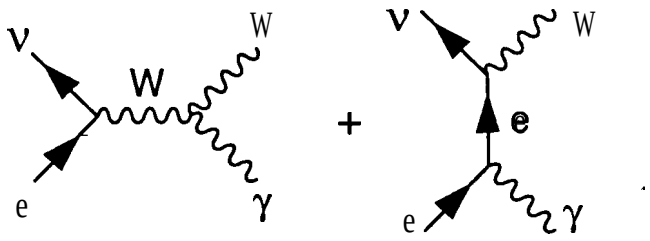

6-89 6383A3

Fig. 3

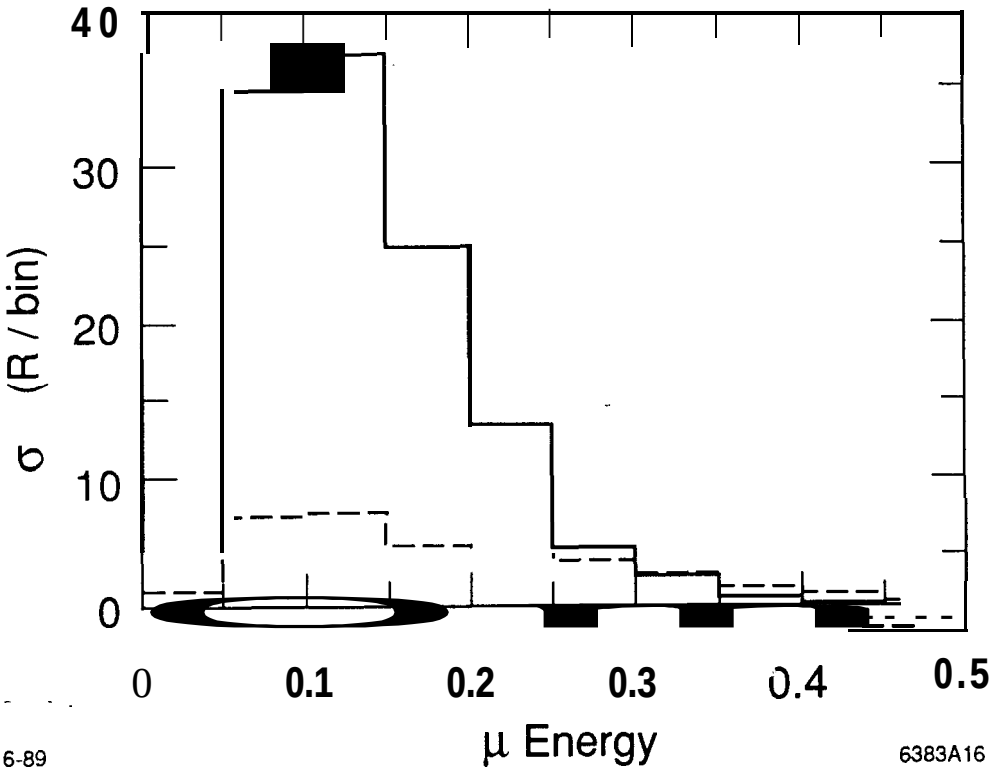

Fig. 4

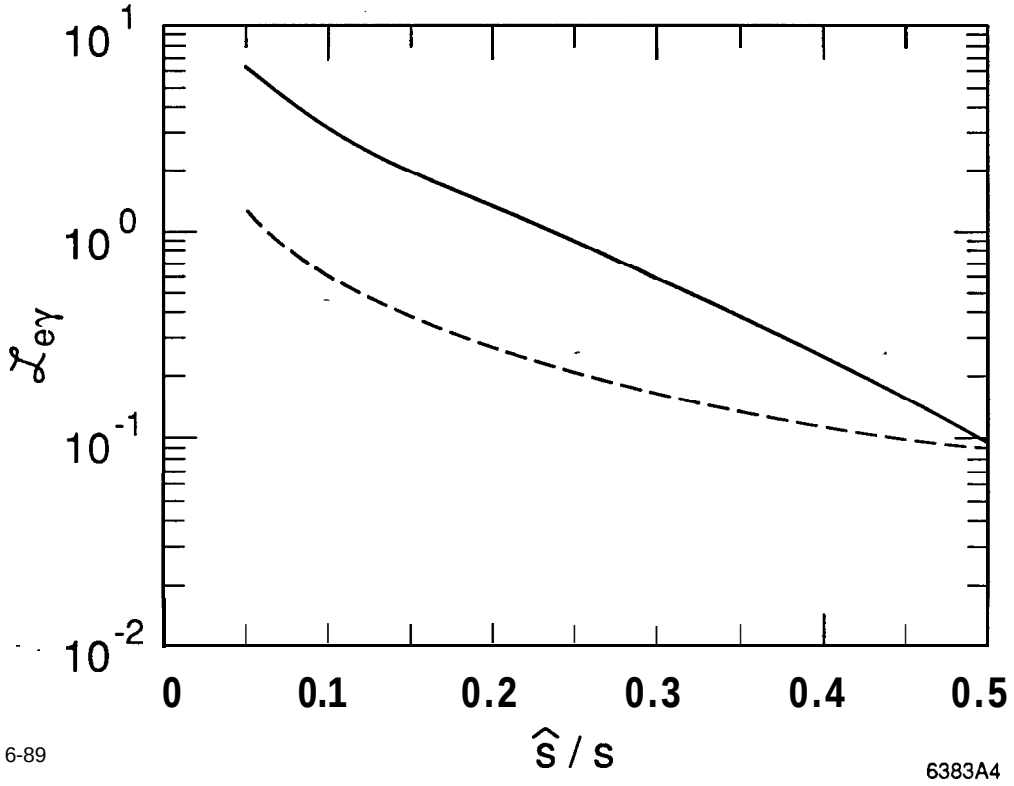
10^1
10^0
10^{-1}
10^{-2}
$\mathcal{L}_{e\gamma}$
0
0.1
0.2
0.3
0.4
0.5
$\hat{s}$ / s
6-89
6383A4

Fig. 5

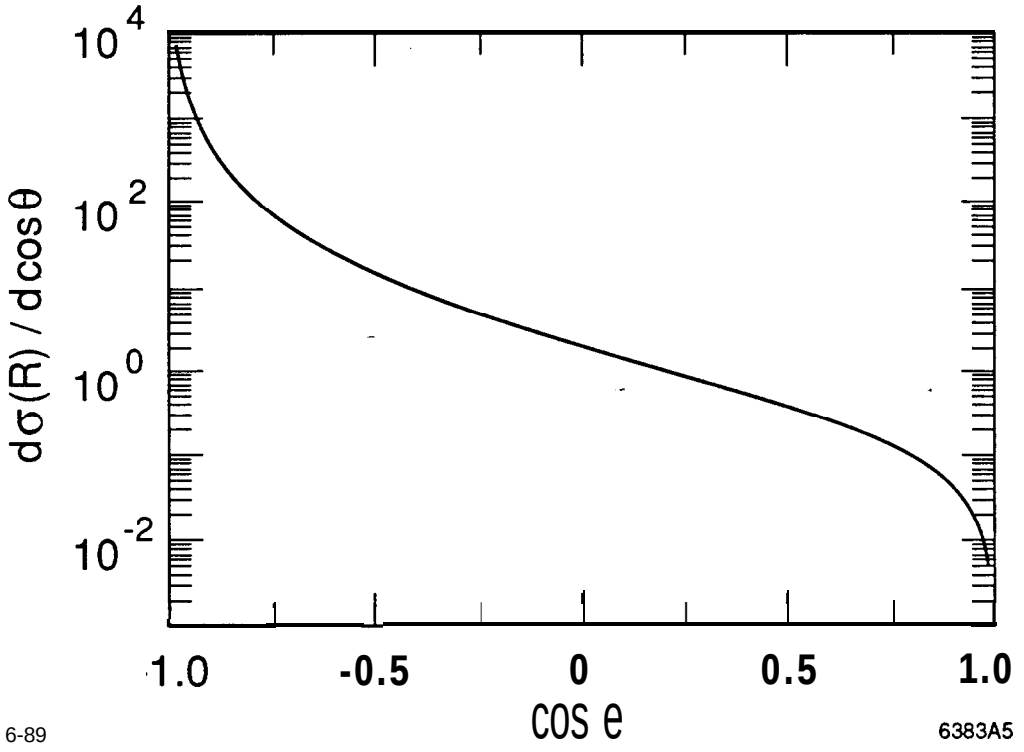
10^4
10^2
10^0
10^{-2}
$d\sigma(R) / d\cos\theta$
-1.0
-0.5
0
0.5
1.0
cos e
6-89
6383A5

Fig. 6

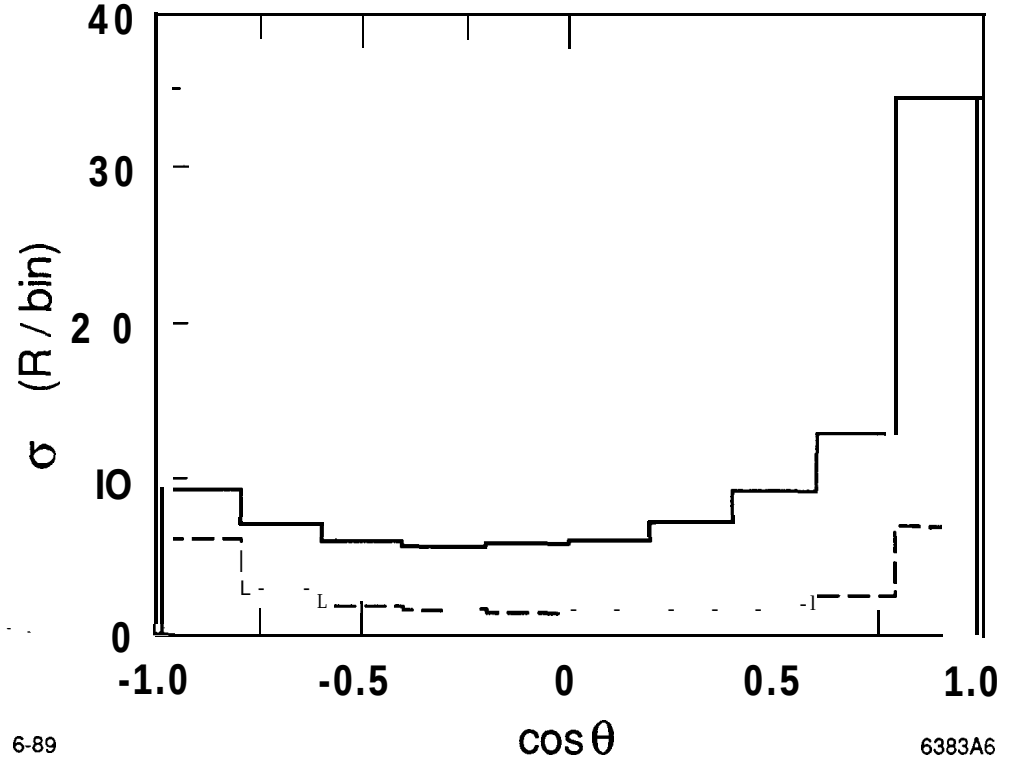

Fig. 7

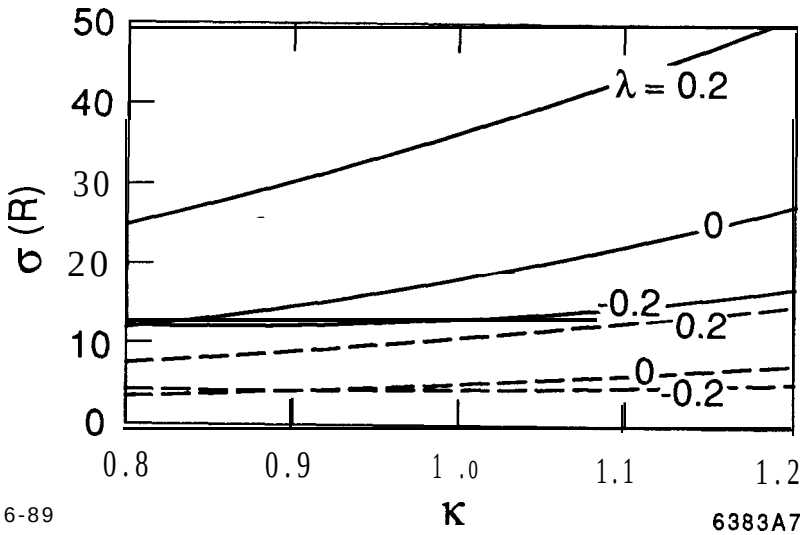

Fig. 8

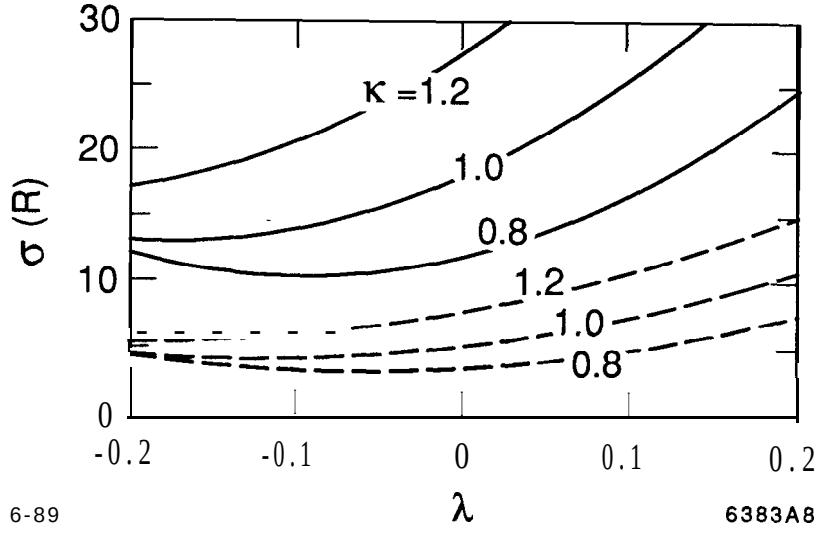

Fig. 9

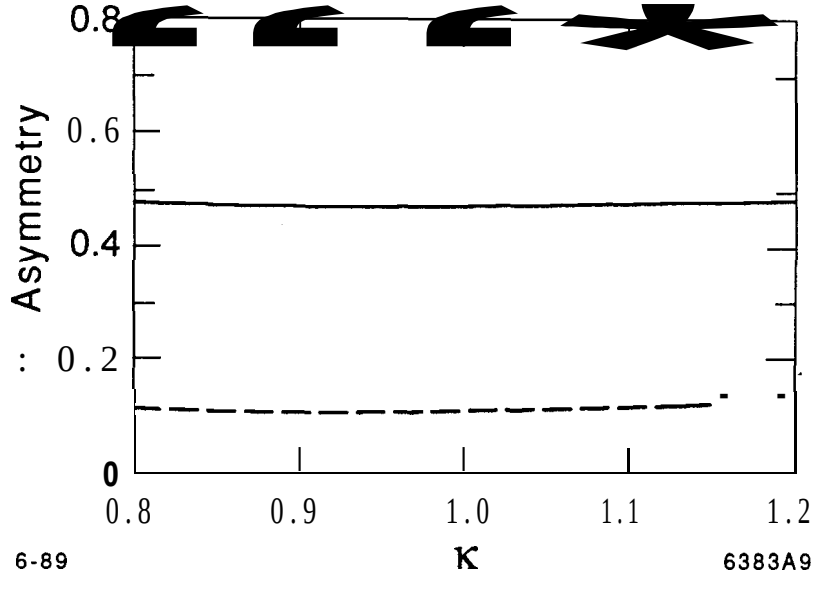

Fig. 10

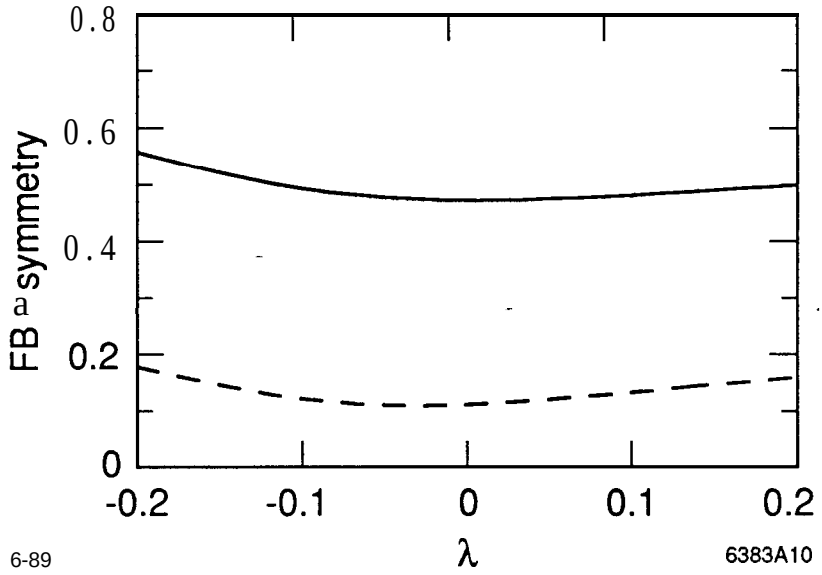

Fig. 11

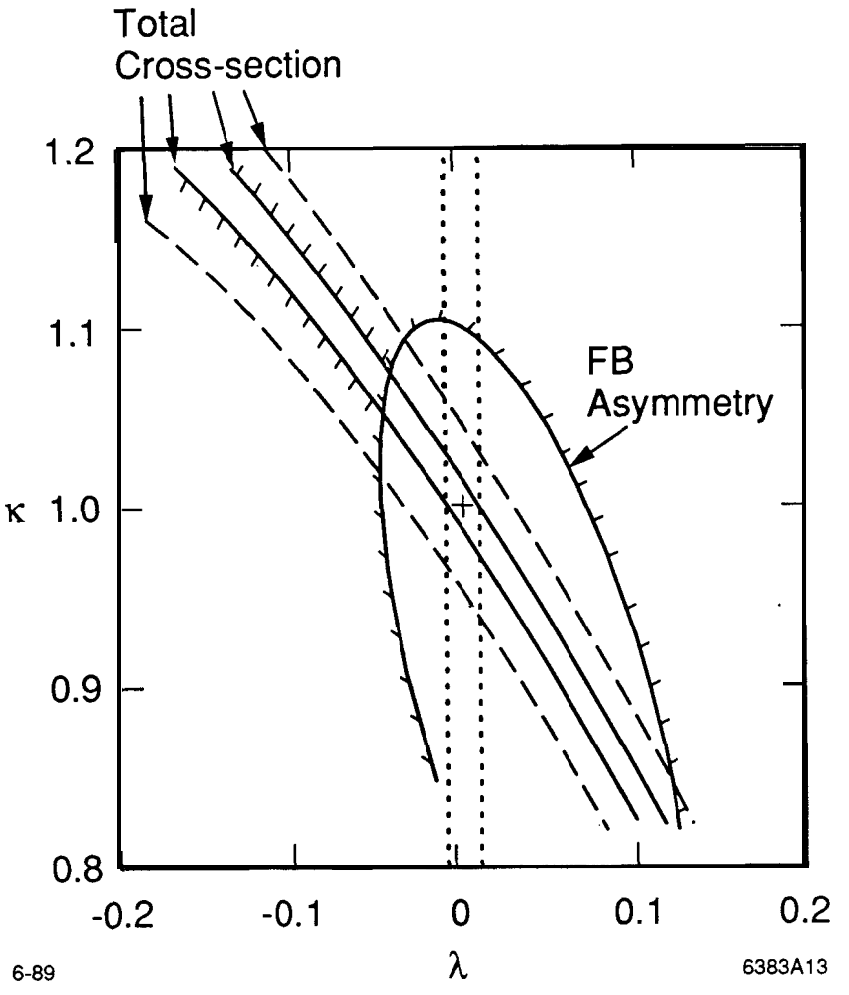
Total
Cross-section
1.2
1.1
1.0
0.9
0.8
κ
FB
Asymmetry
-0.2
-0.1
0
0.1
0.2
λ
6-89
6383A13

Fig. 12

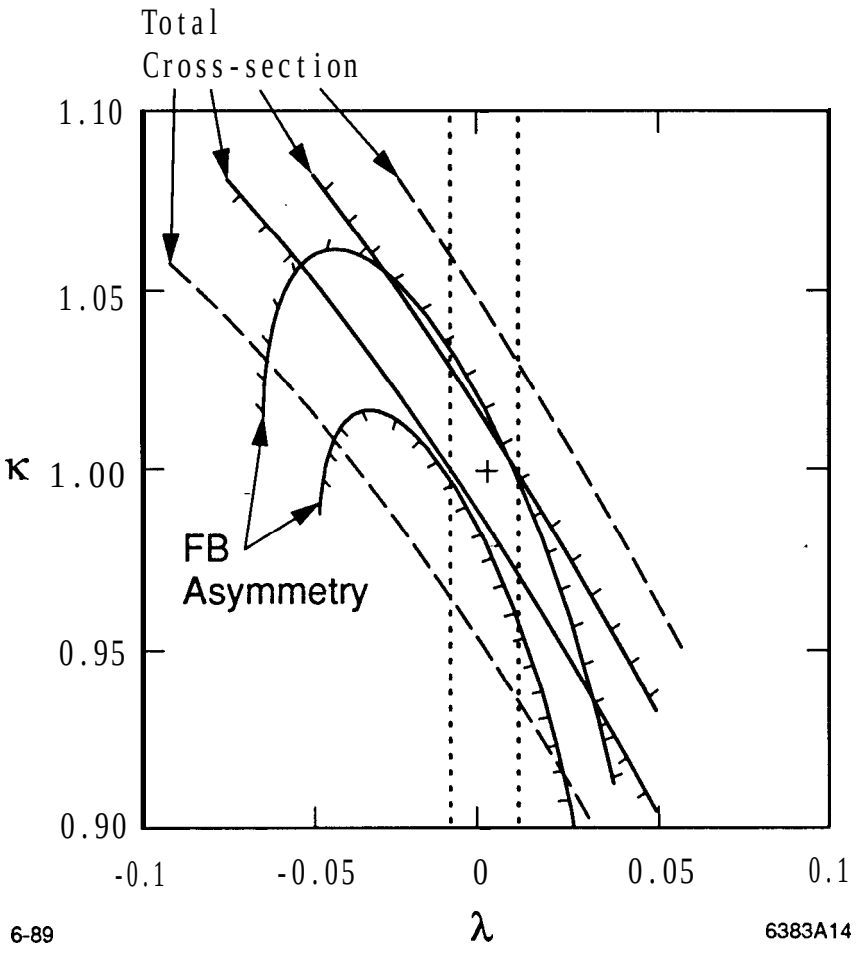
Total
Cross-section
1.10
1.05
κ 1.00
0.95
0.90
FB
Asymmetry
-0.1
-0.05
0
0.05
0.1
λ
6-89
6383A14

Fig. 13